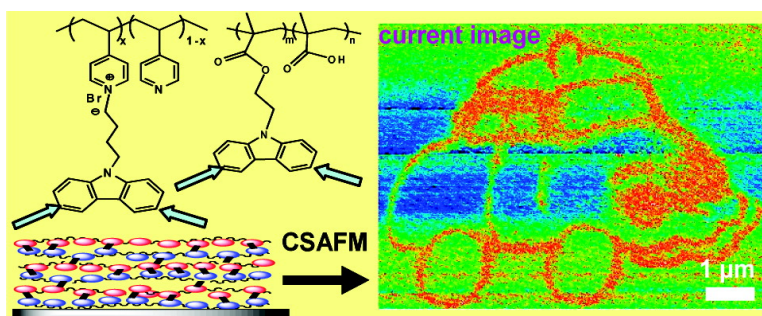


## Electrochemical Cross-Linking and Patterning of Nanostructured Polyelectrolyte/Carbazole Precursor Ultrathin Films

Chengyu Huang, Guoqian Jiang, and Rigoberto Advincula

*Macromolecules*, 2008, 41 (13), 4661-4670 • DOI: 10.1021/ma800268n • Publication Date (Web): 11 June 2008

Downloaded from <http://pubs.acs.org> on December 16, 2008



### More About This Article

Additional resources and features associated with this article are available within the HTML version:

- Supporting Information
- Links to the 1 articles that cite this article, as of the time of this article download
- Access to high resolution figures
- Links to articles and content related to this article
- Copyright permission to reproduce figures and/or text from this article

[View the Full Text HTML](#)

# Electrochemical Cross-Linking and Patterning of Nanostructured Polyelectrolyte–Carbazole Precursor Ultrathin Films

Chengyu Huang, Guoqian Jiang, and Rigoberto Advincula\*

Department of Chemistry and Department of Chemical Engineering, University of Houston, Houston, Texas 77204

Received February 5, 2008; Revised Manuscript Received April 18, 2008

**ABSTRACT:** Nanostructured ultrathin films of pendant carbazole-modified polyelectrolytes were fabricated using the layer-by-layer deposition technique in order to correlate the importance of highly ordered structures and well-defined layer composition in electrochemical cross-linking and nanopatterning. Both UV–vis and surface plasmon resonance (SPR) spectroscopy studies indicated differences in the film structure and bilayer formation based on the degree of electrostatic interaction and carbazole content. Cyclic voltammetry (CV) and SPR studies confirmed the relationship between film structure and the amount of carbazole units per layer affecting the degree of electrochemical cross-linking. CV in particular was used to determine the mechanism of electron transport and electrochemical cross-linking phenomena. Nanopatterning was demonstrated using current sensing AFM (CS-AFM) in which different applied voltages, writing speeds, and composition of polyelectrolytes were studied together with the formation of a complex nanopattern.

## Introduction

In the past decade, polyelectrolytes have attracted considerable attention for the fabrication of nanostructured multilayer ultrathin films.<sup>1</sup> These nanostructured films are constructed by alternating the adsorption of polyanions and polycations to produce multilayer films based on electrostatic attraction. The protocol allows fine control on film composition, architecture, and thickness with nanoscale precision as reintroduced in 1991.<sup>2</sup> The layer-by-layer (LbL) deposition technique is simple yet gives a high degree of control over film complexity.<sup>3</sup> For example, a number of systems have been reported for controlling the growth of polyelectrolyte multilayers,<sup>4</sup> processing,<sup>5</sup> cross-linking, and micropatterning on hydrogen-bonded polyelectrolyte multilayers based on polymer and metal particles.<sup>6</sup> A number of studies have also been reported to have various functionalities such as photoisomerizable films,<sup>7</sup> permselective membranes,<sup>8</sup> and ambipolar field effect transistor behavior,<sup>9</sup> to name a few. Polyelectrolytes have also been used to prepare core–shell and hollow–shell particles using the LbL method.<sup>10–12</sup>

As a class of heteroaromatic organic compounds based on the dibenzopyrrole system, carbazole and its derivatives have been widely studied.<sup>13</sup> Because of its intrinsic fluorescence, it can act as photosensitizer and charge transport material for optoelectronic device applications. The chemical or electrochemical synthesis of polycarbazoles, belonging to a class of electrochemically active semiconducting polymers, has been used for applications such as photovoltaics, OLEDs, and FETs.<sup>14</sup> The most well-known, the 3,6-linked N-substituted carbazole containing polymers, have been extensively studied owing to their interesting electrochemical,<sup>15</sup> electrochromic,<sup>16</sup> electrooptical,<sup>17</sup> and photorefractive<sup>18</sup> properties. On the other hand, the synthesis of 2,7-carbazole-based conjugated polymers have created a new pathway toward achieving efficient luminescence and interesting solvatochromic properties.<sup>19</sup> However, compared to the prevalence of polycarbazoles or other polymers containing carbazole, there have been very few reports on their applications for data storage or memory devices, especially based on electrochemically cross-linked materials.<sup>20</sup> Recently, in our group, a number of studies have been made utilizing carbazole pendant groups as precursors for conjugated polymer network

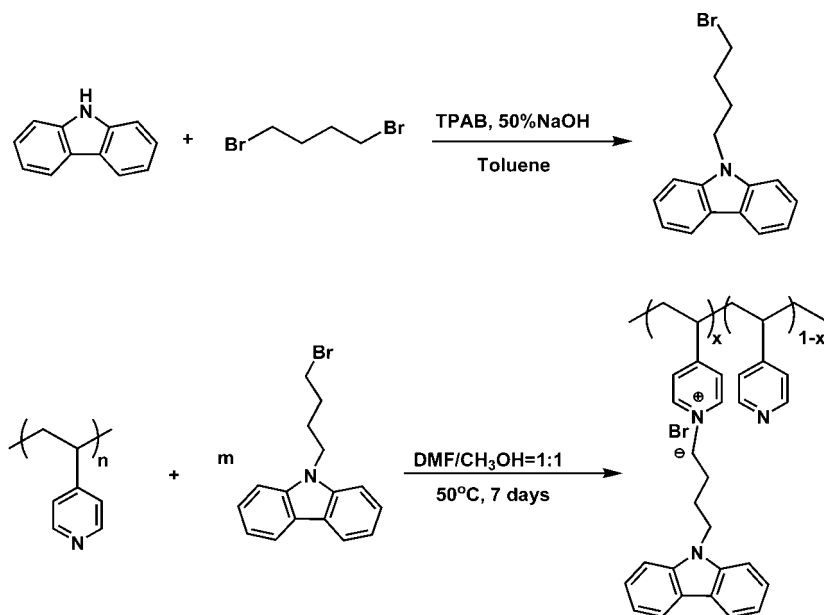
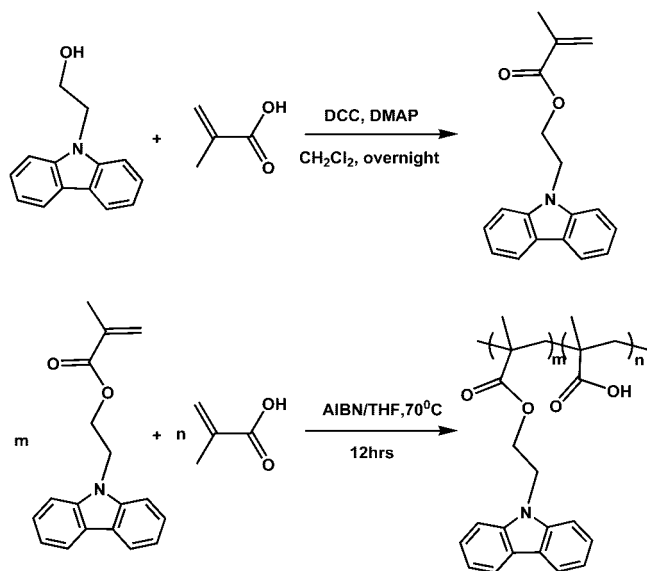
(CPN) formation via electrochemical cross-linking.<sup>21</sup> While most of these studies have been reported from solution or bulk film electrochemical cross-linking, very few reports have been given on the use of layer-by-layer films for CPN formation and nanopatterning.<sup>22</sup>

The focus of this work was on understanding the electrochemical cross-linking and nanopatterning properties of layer-by-layer ordered polyelectrolyte precursors polycarbazoles. An important goal was to quantify this cross-linking behavior with respect to layer order and composition and to demonstrate electro-nanopatterning parameters. A cationic polyelectrolyte precursor, poly[4-(9H-carbazol-9-yl)-N-butyl-4-vinylpyridinium bromide] (P4VPCBZ), based on the quaternization of poly(4-vinylpyridine) (P4VP) was first synthesized. The quaternization reaction and protonation of the nitrogen allowed pairing with an oppositely charged polyelectrolytes through either H-bonding or electrostatic interaction.<sup>23</sup> The cationic polyelectrolyte (shown in Scheme 1) exhibited a pendant electrochemically active carbazole moiety that can undergo chemical oxidation or electrochemical reactions. For the polyanion, a simple procedure involving the partial esterification of the polyacid or copolymerization of acrylic acid and acrylic esters was employed to form poly[2-(N-carbazolyl)ethyl methacrylate-co-methacrylic acid]s (PCEMMAs) as shown in Scheme 2. Alternate multilayer structures of these polyelectrolytes were then deposited using the LbL technique and monitored by a number of spectroscopic methods including surface plasmon resonance (SPR) spectroscopy. Cross-linking of the carbazole groups within the LbL films by cyclic voltammetry (CV) resulted in the formation of a conjugated polymer network (CPN) which is more conducting. Electro-nanopatterning on these films was demonstrated using conducting or current sensing atomic force microscopy (CS-AFM).<sup>24</sup>

## Results and Discussion

**Characterization of the Precursor Polyelectrolytes.** The synthesis and characterization details for the precursor polyelectrolytes P4VPCBZ and PCEMMA are described in the Experimental Section. Two different compositions of the poly(methacrylic acid) copolymers were prepared according to copolymer compositions, PCEMMA32 and PCEMMA41 (ratios of carbazole and carboxylic acid contained units are 3:2 and

\* To whom correspondence should be addressed: e-mail radvincula@uh.edu.

Scheme 1. Synthesis Scheme of Carbazole-Functionalized Poly[4-(9*H*-carbazol-9-yl)-*N*-butyl-4-vinylpyridinium bromide] (P4VPCBZ)Scheme 2. Synthesis Scheme of Poly[2-(*N*-carbazolylethyl methacrylate-*co*-methacrylic acid)s] (PCEMMAs)<sup>a</sup>

<sup>a</sup> Two compositions were made based on the monomers *N*-carbazolylethyl methacrylate:methacrylic acid at 1:1 and 3:2 for PCEMMA32 and PCEMMA41, respectively.

4:1, with feed ratio 1:1 and 3:2 respectively). Instead of being a part of the main chains, the electroactive carbazole substituents were grafted as pendant side groups onto the polymer backbones. The important absorption peaks for carbazole were observed at the 330–333 and 344–347 nm regions, as shown in Figure 1. These peaks are attributed to the  $\pi \rightarrow \pi^*$  and  $n \rightarrow \pi^*$  excitations of the carbazole ring, respectively.<sup>25</sup> Figure 1 also showed convincing evidence that the butylcarbazole was successfully grafted onto the P4VP backbone, which only had an absorption at 267 nm (data not shown). One can also determine the degree of quaternization ( $x$  value as shown in Scheme 1) in the polymer. By using the molar extinction coefficient of the carbazole group, the concentration of carbazole grafted onto the P4VP backbone can be calculated due to the fact that the relative intensities of these peaks increase with increasing molecular weights

of the polymers.<sup>21d</sup> It was determined that  $\sim 61\%$  of the pyridine units were quaternized with the carbazole group.

The materials were then characterized by FTIR. Diagnostic functional peaks were observed such as carbonyl and hydroxy groups of carboxylic acid at 1750 and 3450  $\text{cm}^{-1}$ , respectively, in PCEMMAs as shown in parts c and d of Figure 2. C–O stretching at 1050  $\text{cm}^{-1}$  was also visible for PCEMMAs. PCEMMA32 had a higher intensity of O–H stretching than that of PCEMMA41 since more carboxylic acid functional groups were available within the structure. Besides the C=C of ring in carbazole at 1600  $\text{cm}^{-1}$ , the P4VPCBZ also gave one more peak at 1638  $\text{cm}^{-1}$ , which was assumed to be attributed to the ring of the quaternized pyridine on the chain.

Elemental analysis was carried out to further determine the constitution of the polymer. The amount of carbazole grafted onto the poly(4-vinylpyridine) chain in P4VPCBZ can be calculated according to the following formula:

$$\text{Br fraction} = \frac{[\text{Br}]}{[\text{Br}] + 3[\text{N}]} = x \quad (1)$$

where  $x$  is the normal involved in the P4VPCBZ structure, as shown in Scheme 1, and [Br] and [N] stand for the content of Br and N, respectively. The  $x$  value was found to be 54%, in good agreement with the result from UV–vis calibration in the polymer domain.

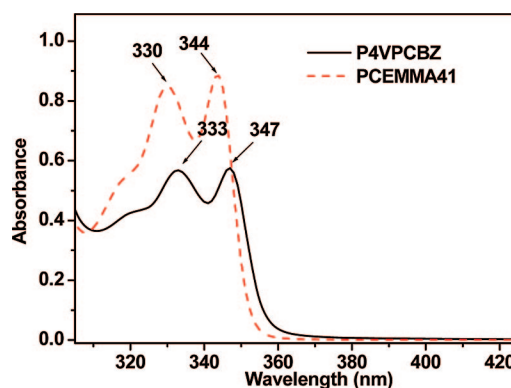
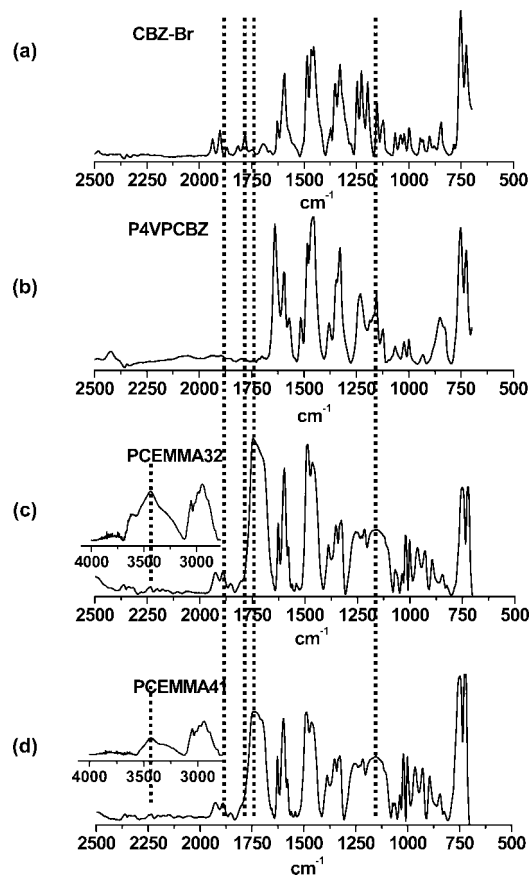


Figure 1. UV–vis spectrum of the P4VPCBZ and PCEMMA41 precursor polyelectrolytes in DMSO. The carbazole peaks are evident at the 330–333 and 344–347 nm regions.



**Figure 2.** FTIR characterization (KBr) of (a) 9-(4-bromobutyl)-9*H*-carbazole (CBZ-Br), (b) poly[4-(9*H*-carbazol-9-yl)-*N*-butyl-4-vinylpyridinium bromide] (P4VPCBZ), and (c, d) poly[2-(*N*-carbazolyl)ethyl methacrylate-*co*-methacrylic acid]s (PCEMMAs, with carbazole/carboxylic acid ratio 3:2 and 4:1).

**Layer-by-Layer Deposition.** LbL deposition on different solid support substrates (quartz, Au-coated glass, or indium tin oxide (ITO) glass) was done by pairing the oppositely charged polyelectrolytes including poly(acrylic acid) (PAA) for control. The deposition processes were monitored *ex situ* by both UV-vis and SPR spectroscopy. The absorbance intensity of each bilayer growth showed a characteristic linear increase (Figure 3). Obviously, the P4VPCBZ/PAA film had the lowest intensity of the carbazole absorption band, which was only present in the P4VPCBZ layers, while the P4VPCBZ/PCEMMAs provided more chromophores originating from both layers. A slight red shift was observed for the P4VPCBZ/PAA film at 347 nm which was not necessarily attributed to aggregation effects. This is reasonable, since PCEMMAs have absorption at 344 nm, which could overlap with the carbazole band of P4VPCBZ. The UV-vis measurement results suggested that the LbL deposition process followed a linear increase, as seen from Figure 3d. According to the polyanion composition by elemental analysis, PCEMMA41 had a larger amount of carbazoles than PCEMMA32, which should lead to more chromophore absorption for the same number of bilayers. Nonetheless, the latter PCEMMA32 had higher absorbance intensity as shown in Figure 3b,d. This might be due to a higher polymer deposition density (chromophore packing/area) or adsorption for this polymer. In PCEMMA41, for every negative charge/carboxylic acid group, four pendant carbazole units occupy more space which effectively decrease the exposure probability of the anionic  $\text{COO}^-$  to the cationic species, leading to a reduced efficiency in forming electrostatic interactions and hence poorer adsorption.

SPR spectroscopy data for the three films are shown in Figure 4. The average thickness for each bilayer was found to be  $0.6 \pm 0.1$ ,  $2.5 \pm 0.3$ , and  $3.2 \pm 0.5$  nm for P4VPCBZ/PAA, P4VPCBZ/PCEMMA32, and P4VPCBZ/PCEMMA41, respectively. The simulation was performed based on the Fresnel equation (Winspall program), with the dielectric constant ( $\epsilon$ ) fixed at 2.5. Because of a higher amount of carbazole units on the polymer chain in the PCEMMAs, they formed thicker bilayers with P4VPCBZ as compared to the P4VPCBZ/PAA film. Also, the weak polyelectrolyte nature of the poly(methacrylic acid) backbone could result in greater conformational freedom or loose structure.<sup>4d</sup> Moreover, the pendant chain could also fill up the volume of the bilayers which is higher for the PCEMMA series. These factors may lead to generally thicker films as compared to the more compact P4VPCBZ/PAA films.

**Electrochemical Cross-Linking.** Cyclic voltammetry has been demonstrated as an effective method to electrochemically cross-link and deposit ultrathin CPN films.<sup>21</sup> The first 10 cycles of the CV traces on the three films with a potential scale from 0 to 1.2 V at a scan rate of 50 mV/s in TBAP/ $\text{CH}_2\text{Cl}_2$  are shown in Figure 5. The oxidation onset at  $\sim 0.95$  V in the first cycle of each film results from the generation of the carbazolium radical cations which allowed further linking of the carbazole units in the films via 3,6 connectivity.<sup>25,26</sup> As the carbazole group cross-linking progressed starting from the second cycle, the CV traces showed an oxidation onset (charging or doping) at about 0.75 V. The oxidation peak current increased in the successive cycles and the increase of charge density with each succeeding cycle are indicative of the formation of higher oligomeric species and further cross-linking.

In general, the rate of redox reactions can be expressed by current density and the rate of electron transfer which is ideally determined by the electron transfer resistance across the conducting polymer film. Since all the CV experimental parameters (scan rate, step width, cross-linking area, etc.) were the same for the three films, the currents should be most likely dependent on the electroactivity of the whole film or even the net content of the carbazole groups per film. In Figure 5 (black curves), the CVs on the P4VPCBZ/PAA film had the lowest current and reached saturation quickly, which seemed to be attributed to the lowest amount of the carbazole pendant groups in the film and the most compact film construction which limited the ion transport through the film. Moreover, the electrochemical cross-linking of the P4VPCBZ/PCEMMA41 film by CV did not lead to the highest current. Instead, the highest oxidation current for the 10 cycles was observed from the P4VPCBZ/PCEMMA32 film. As discussed in an early report, the more carbazole groups were incorporated into the film, the more conjugated polymer film it formed after cross-linking.<sup>26</sup> On the basis of the above observation, it showed a good agreement with the previously measured absorption intensity of the carbazole functional peaks by UV-vis. That is, by using the polyelectrolyte PCEMMA41, the interaction with P4VPCBZ was reduced and the film was not as well packed, which could result in a weaker current, e.g., cross-linking. In general, as compared to the P4VPCBZ/PAA film, the P4VPCBZ/PCEMMA films showed a gradual increase in current upon further cycling, meaning a greater amount of carbazoles/layer were eventually cross-linked. On the other hand, the self-assembled P4VPCBZ/PCEMMA41 film was not only thicker than the P4VPCBZ/PCEMMA32 film but was also found to be rougher morphologically as evidenced by the broader SPR angular curves as well as from the AFM topographic images.

In order to understand the cross-linked films properties in greater detail, potential sweeping was applied with a wider range, from 0 to 1.5 V, while all other parameters were kept the same as those in the previous work. An attempt was made

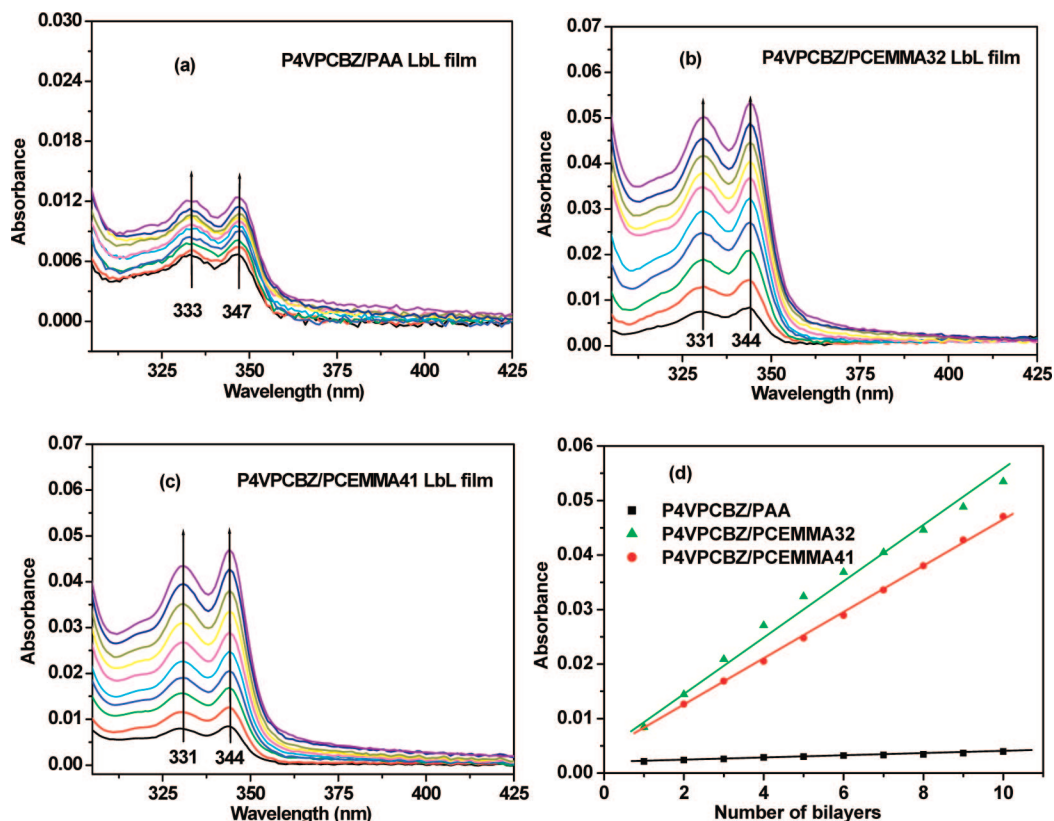


**Figure 3.** Layer-by-layer deposition processes of three types of films as monitored by UV-vis spectroscopy: (a) P4VPCBZ/PAA film, (b) P4VPCBZ/PCEMMA32 film, (c) P4VPCBZ/PCEMMA41 film, and (d) linear plot of film UV-vis absorbance at 344 nm (347 nm for the P4VPCBZ/PAA film).

to completely cross-link all of the carbazole groups by stopping at the higher potential (1.5 V). As shown in Figure 5 (red curves), a new anodic peak at 1.28 V appeared, showing the entire window of the oxidation of carbazole monomers. The polycarbazole doping-dedoping processes were also observed at 0.97 V. The P4VPCBZ/PAA film had very small increase of the oxidation current while P4VPCBZ/PCEMMA films showed apparently gradual increase upon carbazole cross-linking. It is because the P4VPCBZ/PCEMMA films were relatively thicker and had more carbazole groups per bilayer, indicating more cycles were needed to fulfill the complete cross-linking of the whole films. Furthermore, how much the current can increase after a certain cycle before they reach saturation also depends on the different polyanions (weak or strong) in the films. This is because the nature of the polyanions, to some extent, determines the assembly properties of the LbL films such as film porosity and thickness.

Interestingly, after examining the CV traces with 1.2 and 1.5 V as the stopping potentials, we found that there were two changes with respect to the oxidation peaks. Firstly, the whole set of the first oxidation peaks due to the doping effect shifted to lower potential when 1.5 V was applied, especially for the P4VPCBZ/PCEMMA films, as shown in Figure 5. Secondly, in the case of the P4VPCBZ/PCEMMA films, when the potential scans from 0 to 1.2 V were applied, the first oxidation peak moved to a higher potential with increasing number of cycles. In contrast, it shifted to lower potential if the range 0–1.5 V was chosen. Although the mechanism is still not clear, a preliminary explanation is offered as follows: at the lower stopping potential (1.2 V), only a certain amount of carbazoles very close to the anode were oxidized, indicating that the cross-linked compact network could prohibit, to a large extent, the further electron transfer from the electrolyte to the electrode. Thereafter, a higher potential was required to ensure the

occurrence of effective doping and further electrochemical cross-linking. While in the case when 0–1.5 V was applied, partial cross-linking of carbazole through out the whole film probably occurred first. As more cross-linkers formed in the whole film, the energy band gap between HOMO and LUMO decreased continuously, leading to the lower potential needed to oxidize the remaining un-cross-linked carbazole moieties. This was supported by the UV-vis spectra, which showed a 1–2 nm red shift for P4VPCBZ/PCEMMA films after cross-linking of the films.

The cyclic voltammograms of the three types of films after being completely cross-linked in precursor polymer-free solution of 0.1 M TBAP/CH<sub>2</sub>Cl<sub>2</sub> at various scan rates are demonstrated in Figure 6. The currents of the oxidation peaks were dependent on scan rates in the range 50–300 mV/s. The electron transfer rate depends on the electron transfer resistance across the electrode/conductive polymer/electrolyte layer model. The P4VPCBZ/PAA film exhibited a very good linear relationship between  $I$  and  $\nu^{1/2}$ , meaning the films' electron transport was diffusion-limited. The slope of the plot is relative to the number of electrons in unit volume ( $n$ , cm<sup>-3</sup>), diffusion coefficient ( $D$ , m<sup>2</sup>/s), and concentration of electrolyte ions ( $C_0$ , mol/cm<sup>-3</sup>), etc., as indicated by the Cottrell equation:<sup>27</sup>

$$I(t) = \frac{nFAD^{1/2}C_0}{\pi^{1/2}t^{1/2}} \quad (2)$$

For the P4VPCBZ/PCEMMA41 film, it showed a slight departure from the diffusion-controlled behavior, while P4VPCBZ/PCEMMA32 deviated slightly more. This phenomenon is presumably due to the overall structure of the films. In the P4VPCBZ/PAA film, the interstitial spaces were probably large enough for the supporting ions (ClO<sub>4</sub><sup>-</sup>) to penetrate the film and move to the working electrode. Nonetheless, as more

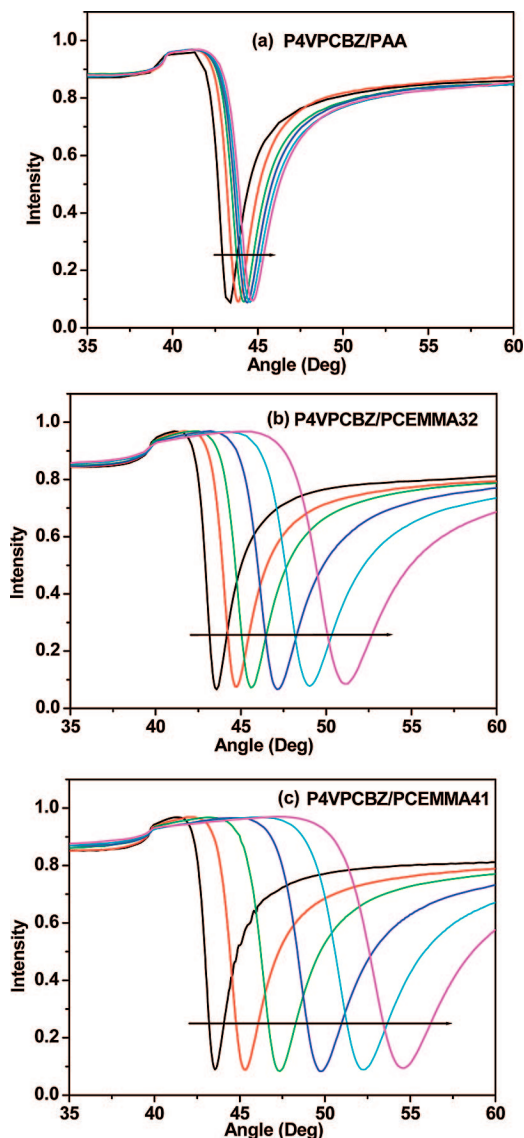


**Figure 4.** SPR reflectivity–angular shifts (p-polarized HeNe at 632.8 nm) after deposition of each two bilayers of the corresponding polyelectrolytes. Films monitored here are (a) P4VPCBZ/PAA, (b) P4VPCBZ/PCEMMA32, and (c) P4VPCBZ/PCEMMA41.

carbazole units were cross-linked, the interstitial spaces within the film become less or smaller, preventing effective  $\text{ClO}_4^-$  transport through the film. Thus, ion transport might become the rate-determining step (RDS) in the electrochemical process. The difference between P4VPCBZ/PCEMMA32 and P4VPCBZ/PCEMMA41 is due to the more effective cross-linking with the former as can also be seen by the higher current increase with increasing scan rate. Thus, the P4VPCBZ/PCEMMA32 film may prove to be the most ideal structure with respect to controlled cross-linkability and feasibility of CPN film formation.

**Nanopatterning.** One of the major applications for semiconducting polymer films is the potential for high-density information storage or memory devices. Many techniques have been developed to explore a robust, easy, fast, and controllable method toward the realization of applicable devices.<sup>28</sup> Herein, we utilized current sensing atomic force microscopy (CS-AFM) to investigate the nanopatterning on the precursor polyelectrolyte-based LbL films and examine the effects of applied bias, writing speed, and film composition on the patterning outcome. The 10-bilayer P4VPCBZ/PAA film on the Au-coated substrate was first chosen as it was relatively smoother. Figure 7a showed

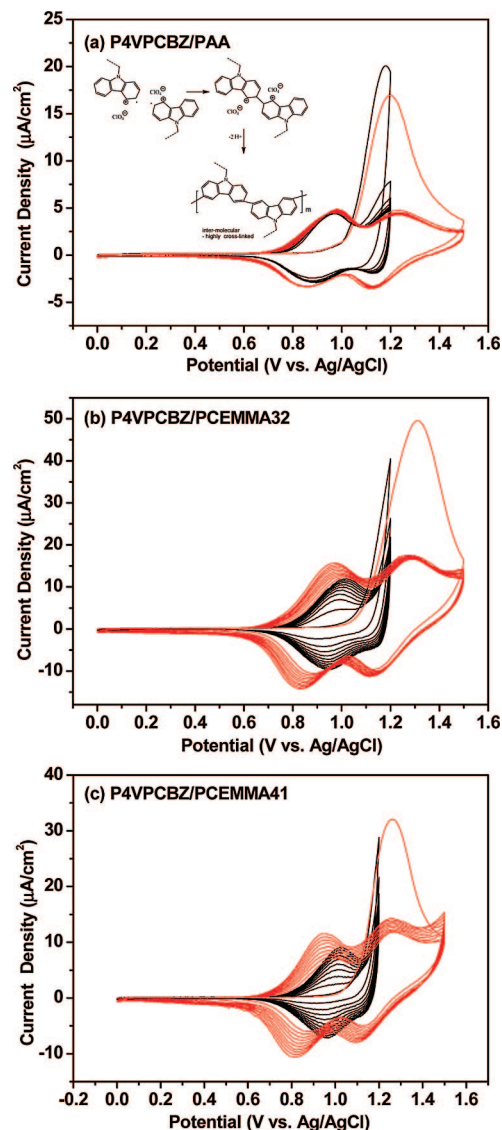


**Figure 5.** The first 10 cycles of the CV traces on the 10-bilayer films of (a) P4VPCBZ/PAA, (b) P4VPCBZ/PCEMMA32, and (c) P4VPCBZ/PCEMMA41 with ITO as the substrate with sweeping between two ranges: (black) 0–1.2 V and (red) 0–1.5 V. Scan rate of 50 mV/s in TBAP/ $\text{CH}_2\text{Cl}_2$  with Pt plate as counter electrode and Ag/AgCl as reference electrode.

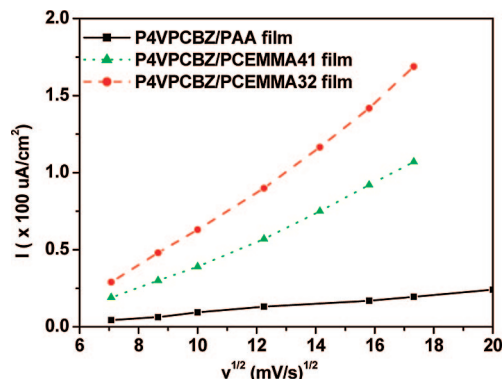


**Figure 6.** Current–scan rate dependence of the three films. The current was calibrated to unit area and was expressed as a function of square root of the scan rate.

the 3D topographic image obtained by applying a constant voltage bias (10 V) at different writing speed ranging from 0.2, 0.4, 0.6 to 0.8  $\mu\text{m}/\text{s}$  (from left to right). The relative heights of

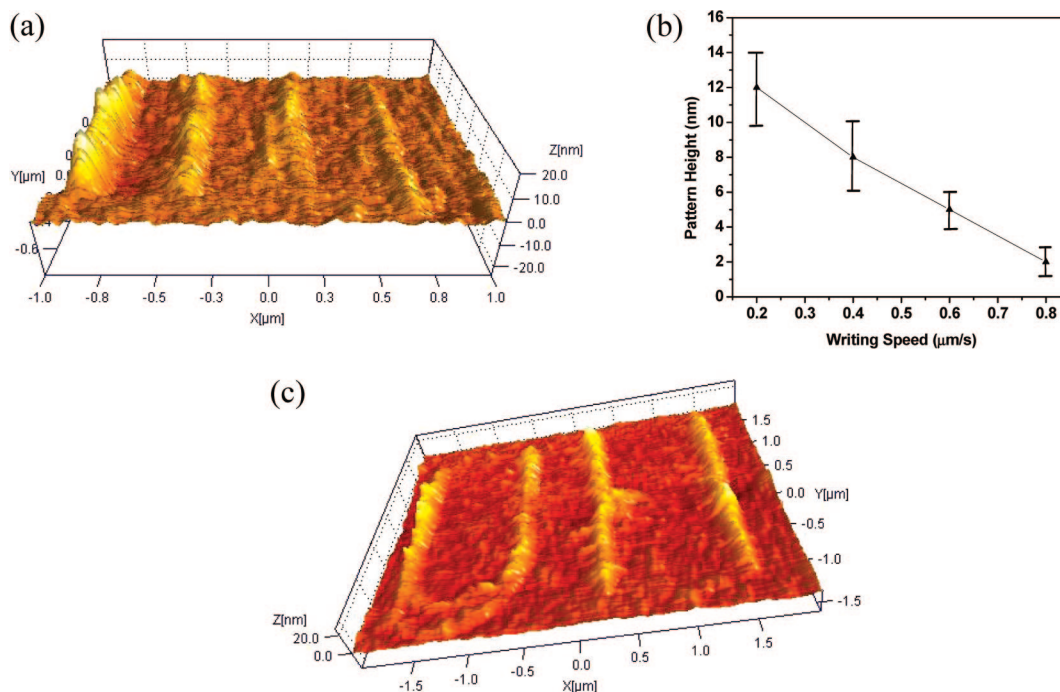


**Figure 7.** Patterning on the 10-bilayer P4VPCBZ/PAA film studied by CS-AFM: (a) 3D topographic image of 4 line patterns after applied 10 V at writing speeds of 0.2, 0.4, 0.6, and 0.8  $\mu\text{m/s}$  (from left to right) with relative heights of  $12 \pm 2$ ,  $8 \pm 2$ ,  $5 \pm 1$ , and  $2 \pm 1$  nm (from left to right), respectively. (b) Plot of the line pattern height as a function of writing speed. (c) "UH" pattern after applying 8 V and 0.4  $\mu\text{m/s}$ .

the line patterns were determined using AFM profilometry with the corresponding lines and was found to be  $12 \pm 2$ ,  $8 \pm 2$ ,  $5 \pm 1$ , and  $2 \pm 1$  nm, corresponding to the writing speeds of 0.2, 0.4, 0.6, and 0.8  $\mu\text{m/s}$ , respectively. The pattern height was highly reproducible from run to run under ambient conditions (22 °C and 50–60% relative humidity). The dependence of pattern height as a function of writing speed is shown in Figure 7b. From the results, it suggests that at a constant voltage bias the height of the line patterns decreased with increasing writing speed in a linear manner. Consequently, the contact time between the conductive tip and the specific location of the precursor polymer film exhibited good control over pattern height. In other words, with fixed applied bias, at lower writing speeds, higher nanopatterns can be expected. The previous investigation showed a similar relationship between the pattern height and tip contact time, in which spin-coated PVK films were used to form nanopatterns under a constant bias.<sup>29</sup> However, no corona pattern formation was observed even at longer residence tip time or slower speed, which behaved differently from a recent study.<sup>30</sup>

To further understand the reliability and reproducibility of patterning on these films, a constant sample bias (8 V) and writing speed (0.4  $\mu\text{m/s}$ ) were applied to prepare a "UH" nanopattern. The height observed was  $7 \pm 3$  nm. The width of each line was determined to be  $196 \pm 14$  nm with high resolution. By comparing the heights of the four different lines in Figure 7a and the "UH" pattern with the same writing speed of 0.4  $\mu\text{m/s}$ , it was found that the height of the "UH" pattern (8 V) is slightly lower than that of the second line in Figure 7a (10 V, from left). This difference is likely due to the lower applied bias. In order to compare the influence of applied voltage on the P4VPCBZ/PAA film in the future, studies will be carried out by utilizing different sample bias on the surface at a constant writing speed.

Aiming to compare the nanopatterning behavior with another precursor polyelectrolyte LbL system, we then used the films containing P4VPCBZ and PCEMMA32 in which both layers have pendant carbazole groups. The patterning on the 10-bilayer

P4VPCBZ/PCEMMA32 film was first attempted by applying a constant bias and varying the writing speed. The 3D image of the line patterns after applying 10 V with increasing the writing speed from 0.2, 0.4, 0.6 to 0.8  $\mu\text{m/s}$  is shown in Figure 8a. The height for each line was determined to be  $15 \pm 3$ ,  $11 \pm 2$ ,  $6 \pm 2$ , and  $2 \pm 1$  nm from left to right. Again, as we can see from Figure 8b, the line pattern height showed a good linear response to the writing speed. The height of each line pattern on P4VPCBZ/PCEMMA32 was found to be slightly higher than that on the P4VPCBZ/PAA film under the same conditions (10 V and the same writing speeds). As mentioned previously, the thickness of the 10-bilayer P4VPCBZ/PCEMMA32 film is about 25 nm, which is roughly 4 times as thick as the 10-bilayer P4VPCBZ/PAA film. Previous investigation has demonstrated that the thickness of the ultrathin films played an important role in controlling the pattern heights due to the change of the electric field inside the LbL films.<sup>31</sup> Given that electrostatic nanolithography is responsible for nanopattern formation, at the same voltage and writing speed, lower pattern heights should be expected from this thicker film. However, as the amount of carbazole groups increases in the P4VPCBZ/PCEMMA32 LbL film, there is a greater possibility for electrochemical cross-linking or/and doping to occur, leading to higher patterns. This is a direct proof that electrostatic patterning mechanism is not the only factor affecting the formation of the protruded patterns.

Figure 9 shows the six-line pattern after applying 8 V with writing speed ranging from 0.2 to 0.7  $\mu\text{m/s}$  or 0.1  $\mu\text{m/s}$  interval. The height for each line was calculated to be  $7.0 \pm 1.2$ ,  $5.0 \pm 1.1$ ,  $3.5 \pm 1.3$ ,  $3.3 \pm 1.3$ ,  $3.1 \pm 1.1$ , and  $2.1 \pm 0.6$  nm, which also presented a clear trend in the height decrease along with increasing the writing speed, although not very linear. Compared to the P4VPCBZ/PCEMMA32 film, the morphology of the LbL the P4VPCBZ/PCEMMA41 film was rougher (even with annealing) so that the nanopatterning on the surface was not as good as expected. A much more amorphous surface than that on the P4VPCBZ/PAA and P4VPCBZ/PCEMMA32 LbL films was observed as examined by AFM, which was consistent with the SPR results of the layer-by-layer films showing broader

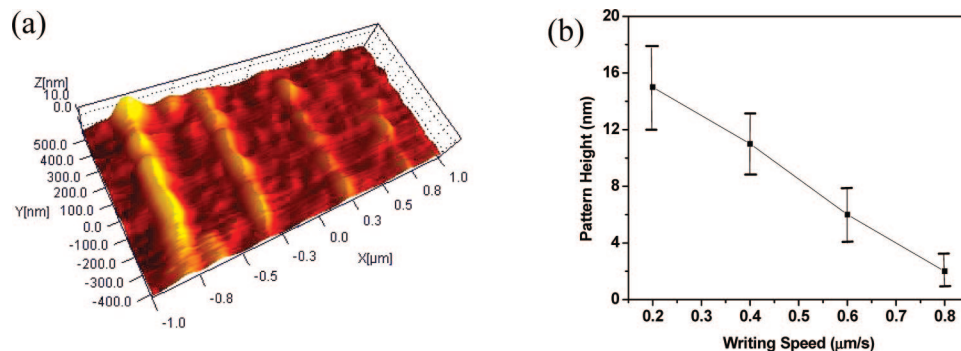


**Figure 8.** Patterning on the 10-bilayer film of P4VPCBZ/PCEMMA32: (a) 3D topographic image of four lines pattern after applying 10 V at different writing speeds of 0.2, 0.4, 0.6, and  $0.8 \mu\text{m/s}$  (from left to right) with the height of each line at  $15 \pm 3$ ,  $11 \pm 2$ ,  $6 \pm 2$ , and  $2 \pm 1$  nm, respectively. (b) Plot of the line pattern height as a function of writing speed.

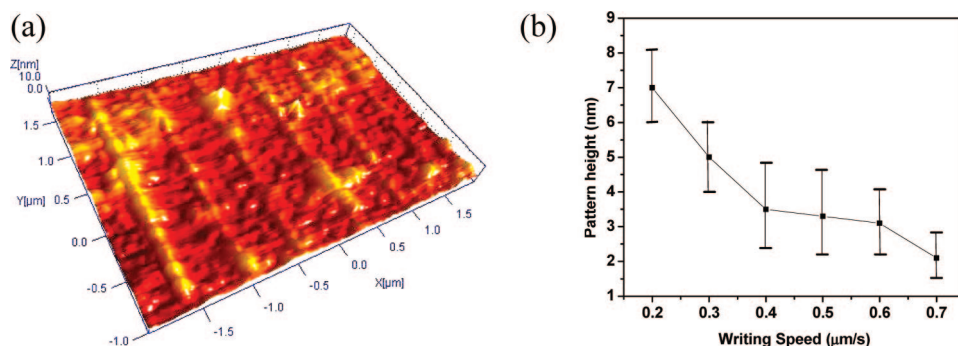


**Figure 9.** Patterning on the 10-bilayer film of P4VPCBZ/PCEMMA32: (a) 3D topographic image of six lines pattern after applying 8 V at different writing speeds of 0.2, 0.3, 0.4, 0.5, 0.6, and  $0.7 \mu\text{m/s}$  (from left to right), and the height for each line is  $7.0 \pm 1.2$ ,  $5.0 \pm 1.1$ ,  $3.5 \pm 1.3$ ,  $3.3 \pm 1.3$ ,  $3.1 \pm 1.1$ , and  $2.1 \pm 0.6$  nm, respectively. (b) Plot of the line pattern height as a function of writing speed.

surface plasmon curves. The linear charge density of the polyelectrolytes is a very important factor in controlling LbL film properties since the polyelectrolyte adsorption is driven by electrostatic interactions. Rubner and Jonas<sup>32,33</sup> have reported that the growth of LbL multilayers based on weak polyelectrolytes such as poly(acrylic acid) (PAA) and poly(allylamine) (PAH) are pH dependent due to the varying ionization degrees. It was observed that the surface wettability, the level of layer interpenetration, the thickness, and the surface roughness of the films were sensitive to the linear charge density of the polyelectrolytes, which was varied by changing the pH of the dipping solutions.

The mechanism for the nanopatterning process can be attributed but not limited to a combination of several different factors, such as electrostatic nanolithography, joule heating, anion doping, or/and electrochemical cross-linking of carbazole functional groups. First, it is known that the electric field ( $E$ ) across the whole thin film is correlated to the sample bias ( $V$ ) and the distance ( $d$ ) between the AFM conducting tip and the conducting substrate. Lyuksyutov et al.<sup>34</sup> studied electrostatic nanolithography on polymethyl methacrylate (PMMA) and polystyrene (PS) spin-coated films with a relatively strong nonuniform electric field ( $10^8$ – $10^{10}$  V/m). The electrical conductivity (increased resistance) between the conductive tip and the polymer was strong enough to drive the softened material toward the tip with  $T > T_g$ , leading to the raised features. In our work, the electric field was estimated to be  $\sim 10^9$  V/m; therefore, the electrical conductivity should be taken into account in describing the possible mechanism for the nanopattern formation. Second, localized joule heating was likely to occur due to the current flow through the dielectric thin film in the high electric field region. Lastly, electrochemical cross-linking of the electroactive groups and anion doping of the conjugated polymers under the external applied bias played an

important role in the formation of nanopatterns. Very recently, in our group, CS-AFM has been used to fabricate memory device/data storage on the basis of anion doping of semiconducting polymer ultrathin films.<sup>31,35</sup> Anions such as  $\text{HCO}_3^-$  and  $\text{OH}^-$  in the water meniscus can be doped into the polymeric film when the semiconducting material was loaded with a certain bias in the proper direction. Jegadesan et al.<sup>29,30</sup> utilized CS-AFM to study the nanopatterning on carbazole monomer and PVK spin-cast ultrathin films, and the electrochemical cross-linking of carbazole was confirmed by measuring the  $I$ – $V$  properties on the patterned domains. Xie<sup>36</sup> has reported nanopatterning with distinct physical and chemical characteristics by tuning the magnitude and duration of nanodischarge.

Finally, a more complex pattern was drawn in order to demonstrate the facile patterning on these types of LbL films. Figure 10 showed the 2D topographic and current images of a “nanocar” written at 10 V with a writing speed of  $0.8 \mu\text{m/s}$  on the 10-bilayer P4VPCBZ/PAA film. The average height of the pattern was determined to be 2.4 nm, which is consistent with that of the fourth line in Figure 7a (from left to right, 10 V,  $0.8 \mu\text{m/s}$ ). The current image, as shown from Figure 10b, was obtained under 1 V sweeping of the film after the patterning. It is clearly seen that the orange-brown color contour showed a higher current flow through the “nanocar” pattern. In another words, the conductivity of the “nanocar” is higher than the unpatterned domains. This indicated the occurrence of anion doping or/and electrochemical cross-linking at patterned regions of the polymer film. On the basis of the reported literature and our previous studies,<sup>24,29–31,34,35</sup> we believe the patterning mechanism can be explained as follows. Under a certain sample bias, the strong electric field ( $10^8$ – $10^{10}$  V/m) between the conducting AFM tip and the substrate generates a significant joule heating locally which softens the dielectric material. Meanwhile, the softened polarizable material flows toward the

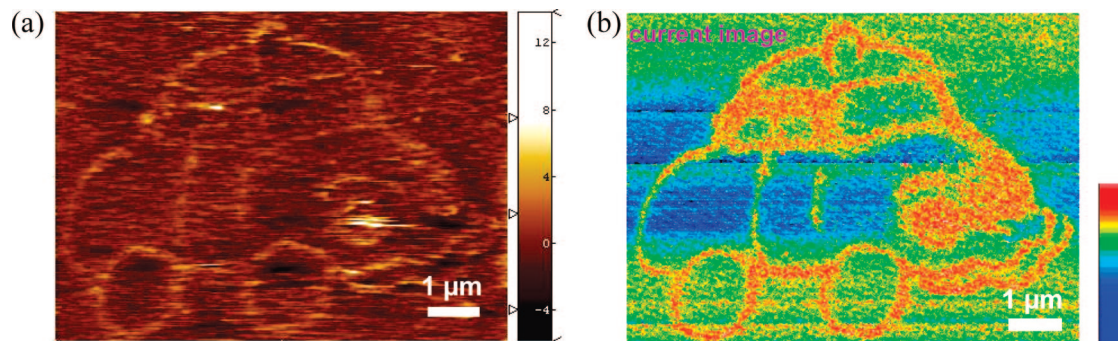


**Figure 10.** CS-AFM nanopatterning of a “nanocar” on a 10-bilayer P4VPCBZ/PAA film at 10 V with a writing speed 0.8  $\mu\text{m/s}$  (a) topographic image and (b) current image. The current image was obtained by scanning at 1 V after the patterning. Color bar range is 0–14.7 pA.

tip (mass transport) under strong electric field with the assistance of water meniscus as a bridge. This process eventually leads to the raised features. Additionally, the carbazole units undergo oxidation and cross-link with each other, forming CPN species under the applied bias. The water meniscus is dissociated into some small ion species by the strong electric field, which acts as a supporting electrolyte for the carbazole electrochemical cross-linking. Moreover, the anionic species in the water meniscus move into the film (doping/charging, ion transport), leading to the enhanced conductivity over the raised features. Future work should be focused on the patterning under different conditions such as writing speed, applied voltage, and humidity. Furthermore, quantification of the conductivity enhancement after nanopatterning from  $I$ – $V$  characteristics is required. As a control, before nanopatterning, a fully cross-linked LbL film can be prepared electrochemically until there is no more increase with respect to the oxidation current. In this case, the doping level of the film should be maximized. If the conductivity on the patterns before and after patterning shows no distinguishable change, this can prove that anion doping indeed responsible for the current increase.

## Conclusion

The synthesis of pendant carbazole-modified polyelectrolytes and their application as ultrathin films have been demonstrated using the layer-by-layer deposition technique. Both UV–vis and SPR studies showed differences in the film structure and bilayer formation based on electrostatic interaction and carbazole content. Essentially the weaker polyelectrolyte poly(methacrylic acid) copolymerized with the carbazole containing polymer, resulting in thicker films. The CV and SPR studies indicated that the electrochemical behavior was related to the film structure and the amount of carbazole units per layer. The electron transport and doping properties were also found to be dependent to the degree of electrochemical cross-linking. CV studies suggested that the electrochemical cross-linking of the LbL films resulted in an electron transport behavior which was diffusion limited. These films were subsequently employed for the investigation of electrochemical nanopatterning using current sensing AFM as a writing technique. The dependence of the nanofeature properties on applied voltage, writing speed, and composition of the polyelectrolytes was studied together with the mechanism. The pattern formation was demonstrated in order to show the possibility for future applications such as information storage devices.

## Experimental Section

**Chemicals.** Poly(4-vinylpyridine) (Aldrich, MW ca. 60 000), 1,4-dibromobutane (Aldrich, 99%), tetrapropylammonium bromide (Acros, 98%), 9*H*-carbazole-9-ethanol (Aldrich, 95%), *N,N'*-dicyclohexylcarbodiimide (DCC, Acros, 99%), 4-(dimethylamino)py-

ridine (DMAP, Aldrich, 99%), PAA (Aldrich, typical MW = 2000 (GPC)), tetrabutylammonium perchlorate (TBAP, Strem, minimum 98%), 3-mercaptopropanesulfonate (Aldrich, 90%), 3-aminopropyltriethoxysilane (APS, Aldrich, 99%),  $\text{Na}_2\text{SO}_4$ , NaOH, and HCl were used as received. Carbazole (Aldrich, 96%) and 2,2'-azobis(isobutyronitrile) (AIBN, Aldrich, 98%) were recrystallized twice from ethanol. Methacrylic acid (Aldrich, stabilized with ca. 250 ppm MEHQ, 99.5%) was pretreated to remove the inhibitor by passing through a minitype column with inhibitor–remover replacement packing. All solvents were purchased from Aldrich and distilled and dried properly before use.

**Instrumentation.** NMR spectra and  $M_n$  analysis were obtained on a General Electric QE 300 spectrometer (300 MHz). UV–vis spectra were recorded using an Agilent 8453 spectrometer. FTIR was performed on an FTS 7000 FT-IR spectrometer in the 700–4000  $\text{cm}^{-1}$  region (Digilab, now Varian Inc., resolution = 8  $\text{cm}^{-1}$ , filter = 5 kHz). The CV was performed on an Amel 2049 potentiostat and power laboratory/4SP system with three electrodes. The cell contains a 0.1 M TBAP solution in methylene chloride, with a platinum plate as the counter electrode and a Ag/AgCl reference electrode. The thickness and the kinetic of adsorption for layer-by-layer films were measured by in situ surface plasmon resonance (SPR) spectroscopy with gold-coated LaSFN9 glass substrate. The surface plasmon spectra was obtained in the SPS mode of the Multiskop (Optrel GmbH) with the attenuated total reflection (ATR) setup used for the excitation of surface plasmons in the classical Kretschmann configuration. The excitation source employed was a p-polarized He–Ne laser at 632.8 nm. The software WINSPALL was especially used for the fitting of SPR spectroscopy (Knoll group at Max-Planck-Institute (Mainz, Germany) based on the Fresnel equations and the matrix formalism).

**Synthesis.** *Synthesis of 9-(4-Bromobutyl)-9*H*-carbazole.* The synthesis of 9-(4-bromobutyl)-9*H*-carbazole was accomplished by a modification of a procedure reported by Bo et al.<sup>37</sup> A mixture of 10.32 g (61.72 mmol) of carbazole in toluene (100 mL) containing 1,4-dibromobutane (118.2 g, 547.4 mmol), and TPAB (tetrapropylammonium bromide) (3 g) was stirred at 45  $^\circ\text{C}$  for 3 h and then left at room temperature overnight. Methylene chloride was used to extract the product. The eluent was washed with water and brine and dried over  $\text{Na}_2\text{SO}_4$ . After removal of the solvent, the excess 1,4-dibromobutane was evaporated by vacuum distillation. The residue was recrystallized from ethanol to give 16.7 g (89.5%) of the product.  $^1\text{H}$  NMR ( $\text{CDCl}_3$ )  $\delta$  (ppm): 8.27 (d, 2H), 7.52–7.40 (m, 4H), 7.27 (m, 2H), 4.37 (t, 2H), 3.39 (t, 2H), 2.35 (s, 3H), 2.11–2.03 (m, 2H), 1.98–1.90 (m, 2H).

*Synthesis of Poly[4-(9*H*-carbazol-9-yl)-*N*-butyl-4-vinylpyridinium bromide].* A mixture of 0.5965 g (4.412 mmol) of poly(4-vinylpyridine) with MW ca. 60 000 and 2 g (6.618 mmol) of 9-(4-bromobutyl)-9*H*-carbazole in 3.7 mL of DMF/ $\text{CH}_3\text{OH}$  (1:1) was stirred at 50  $^\circ\text{C}$  in a round-bottom flask for 1 week. The mixture became clear after 3 h and then turned red 3 days later. Toluene was used to precipitate the brownish solid product followed by Soxhlet extraction for 3 days, giving 2.4 g (83%) of product after vacuum drying.  $^1\text{H}$  NMR ( $\text{DMSO}-d_6$ )  $\delta$  (ppm): 8.84 (s, broad, 1H),

7.96 (s, 2H), 7.46–7.00 (m, 5H), 4.29 (s, 2H), 2.22–1.70 (m, 5H). This polymer is soluble in DMSO and DMF, but not water. However, a dilute aqueous solution can be prepared by applying drops of DMSO to predissolve the polymer, followed by the proportional ratio of water, to make the desired concentrations.

**Synthesis of 2-(*N*-Carbazolyl)ethyl Methacrylate.** 2-(*N*-Carbazolyl)ethyl methacrylate was synthesized by esterification, as shown in Scheme 2. A mixture of 2-(*N*-carbazolyl)ethanol (10 g, 47.3 mmol), methacrylic acid (4.075 g, 47.3 mmol), and 13.7 g of DMAP (*p*-dimethylamino)pyridine) in anhydrous methylene chloride was kept stirring at 0 °C under nitrogen for at least 15 min. 0.578 g of DCC (dicyclohexylcarbodiimide) was predissolved in methylene chloride and then added dropwise into the stirring mixture. The reaction mixture was warmed to room temperature overnight. After neutralizing with NaHCO<sub>3</sub> (pH = 8) and washing with water, the organic layer was dried over MgSO<sub>4</sub> and recrystallized with methanol, giving 8.3 g (63%) of the product. <sup>1</sup>H NMR (CDCl<sub>3</sub>) δ (ppm): 8.12 (s, 2H), 7.52–7.45 (m, 4H), 7.30–7.24 (m, 2H), 5.95 (s, 1H), 4.63 (t, 2H), 4.55 (t, 2H), 1.82 (s, 3H). <sup>13</sup>C NMR (CDCl<sub>3</sub>) δ (ppm): 167.24, 140.35, 135.62, 126.34, 125.75, 122.98, 120.37, 119.22, 108.59, 62.46, 41.59, and 18.20.

**Synthesis of Poly[2-(*N*-carbazolyl)ethyl methacrylate-co-methacrylic acid]s (PCEMMAs).** The copolymerization was carried out at variable ratio (*m*:*n* = 1:1, 3:2) to form the copolymer structures (PCEMMAs). A 25 mL (20 mL) anhydrous THF solution of 2-(*N*-carbazolyl)ethyl methacrylate (600 mg, 2.148 mmol), 182.2 μL (121.4 μL) of methacrylic acid, and 82.4 mg of AIBN was stirred at 70 °C for 12 h and precipitated with hexane. The yield was 75% (76% for PCEMMA41 with feed ratio 3:2) after vacuum drying. For PCEMMA32, <sup>1</sup>H NMR (DMSO-*d*<sub>6</sub>) major peaks: δ (ppm): 12.35 (br, 0.5H), 8.03 (br, 2H), 7.37–7.11 (br, 5.5H), 4.53–4.27 (br, 3.3H), *M*<sub>n</sub> = 2933. Elem. Anal. Calcd: C<sub>12.4</sub>H<sub>12.6</sub>N<sub>0.6</sub>O<sub>2</sub>. Found: C, 72.56; H, 6.40; N, 4.36; O, 16.68. For PCEMMA41, <sup>1</sup>H NMR major peaks: 12.36 (br, 0.2H), 8.02 (br, 2H), 7.36–7.11 (br, 5.7H), 4.49–4.06 (br, 3H), *M*<sub>n</sub> = 7032. Elem. Anal. Calcd: C<sub>15.2</sub>H<sub>14.8</sub>N<sub>0.8</sub>O<sub>2</sub>. Found: C, 74.00; H, 6.20; N, 5.12; O, 14.68.

**Layer-by-Layer Deposition and Electrochemical Cross-Linking of the Films.** BK7 microscope slides were first cleaned twice using 2% standard ultrasonic cleaning solutions for 15 min, followed by rinsing with abundant Milli-Q water. After sonicating with acetone and Milli-Q water and then drying, a piranha solution (30% hydrogen peroxide, 70% sulfuric acid) was used to further clean the glass surface for 30 min. The slides were finally treated with Ar/O<sub>2</sub> plasma cleaning for further use: functionalization and gold substrate evaporation.

ITO slides were first washed with Alconox by hands and then rinsed with Milli-Q water. The slides were then sonicated in isopropanol, hexane, and toluene for 10 min, followed by treatment with RCA recipe (H<sub>2</sub>O/H<sub>2</sub>O<sub>2</sub>/NH<sub>3</sub>, 10:2:0.6, 55–60 °C, 75 min). After Ar/O<sub>2</sub> plasma treatment, both ITO and BK7 slides were immersed into the silylating bath (0.5 vol % 3-aminopropyltriethoxysilane (APS) in toluene) at 95 °C for 2 h, followed by rinsing with toluene and methanol for 15 min. The slides could be stored in methanol and, before using, 20 min treated in a 1 N HCl solution to positively charge the amino groups.

To prepare gold substrates, the cleaned BK7 slides were fixed onto the holder of the vacuum evaporator. A 1–2 nm thick chromium layer and a 45–50 nm thick gold layer were evaporated on the slides under high vacuum (<6 × 10<sup>-6</sup> Torr) when spinning. The Au/Cr/BK7 slides were then treated with 3-mercaptopropylsulfonic acid, sodium salt (0.2 mg/mL in ethanol), for at least 1 h for surface functionalization.

Promoted layer-by-layer deposition method. Solutions used here were (i) P4VPCBZ, 1 mM in water/DMSO (v:v = 4:1); (ii) rinsing solution, water/DMSO (v:v = 4:1); (iii) rinsing solution, water; (iv) PAA, 1 mM in water (pH = 10) or PCEMMAs, 1 mM, in water/DMSO (v:v = 3:2, pH = 10); (v) rinsing solution, water (pH = 10) or water/DMSO (v:v = 3:2, pH = 10); (vi) rinsing solution, water.

The positively charged polyelectrolyte was made with a concentration of 1 mM P4VPCBZ in water/DMSO (v:v = 4:1). Three

polyanions, 1 mM PAA in H<sub>2</sub>O, 1 mM PCEMMA32, and 1 mM PCEMMA41 in water/DMSO (v:v = 3:2), were used as the negatively charged polymer solutions to seek the influence of the loading of carbazole groups. The alternate deposition was followed by careful rinsing after each immersion. Besides using the original solvent and condition, such as pH value, pure water was also involved as a second rinsing in preparation of each layer to remove any last traces of DMSO and adjust the pH back to neutral.

The deposition process was monitored by UV-vis spectroscopy after the fabrication of LbL films on BK7 slides and by SPR on Au slides. The CV studies were carried out on the as-prepared LbL films to study the electrochemical properties with different potential windows and diverse materials at a scan rate of 50 mV/s. It was performed in a three-electrode cell containing 0.1 M tetrabutylammonium perchlorate (TBAP)-methylene chloride solution, with platinum as the counter electrode and Ag/AgCl as the reference electrode. Copious washing with methylene chloride and drying was performed after film cross-linking.

**Acknowledgment.** The authors acknowledge funding from the Robert E. Welch Foundation (E-1551), NSF DMR-0602896, and the Alliance for Nanohealth of Texas. Technical support from Optrel GmBH, Agilent Technologies (Molecular Imaging), and Varian Instruments Inc. is also acknowledged. Helpful discussions with Dr. Prasad Taraneekar and Dr. Akira Baba are appreciated.

## References and Notes

- (1) (a) Esker, A. R.; Mengel, C.; Wegner, G. *Science* **1998**, *280*, 892. (b) Caruso, F.; Niikura, K.; Furlong, D. N.; Okahata, Y. *Langmuir* **1997**, *13*, 3427. (c) Kotov, N. A.; Dekany, I.; Fendler, J. H. *J. Phys. Chem.* **1995**, *99*, 13065.
- (2) (a) Decher, G.; Hong, J. D. *Makromol Chem., Macromol. Symp.* **1991**, *46*, 321. (b) Decher, G.; Hong, J. D.; Schmitt, J. *Thin Solid Films* **1992**, *210*, 831. (c) Decher, G. *Science* **1997**, *277*, 1232.
- (3) Flores, H.; Menchaca, J. L.; Tristan, F.; Gergely, C.; Perez, E.; Cuisinier, F. J. G. *Macromolecules* **2005**, *38*, 521.
- (4) (a) Lee, I.; Ahn, J. S.; Hendricks, T. R.; Rubner, M. F.; Hammond, P. T. *Langmuir* **2004**, *20*, 2478. (b) Berg, M. C.; Yang, S. Y.; Hammond, P. T.; Rubner, M. F. *Langmuir* **2004**, *20*, 1362. (c) Yoo, D.; Shiratori, S. S.; Rubner, M. F. *Macromolecules* **1998**, *31*, 4309. (d) Li, Z.; Lee, D.; Rubner, M. F.; Cohen, R. E. *Macromolecules* **2005**, *38*, 7876.
- (5) (a) Lee, D.; Rubner, M. F.; Cohen, R. E. *Chem. Mater.* **2005**, *17*, 1099. (b) Zhai, L.; Cebeci, F. C.; Cohen, R. E.; Rubner, M. F. *Nano Lett.* **2004**, *4*, 1349.
- (6) (a) Yang, S. Y.; Rubner, M. F. *J. Am. Chem. Soc.* **2002**, *124*, 2100. (b) Yang, S. Y.; Lee, D.; Cohen, R. E.; Rubner, M. F. *Langmuir* **2004**, *20*, 5978. (c) Yang, S. Y.; Mendelsohn, J. D.; Rubner, M. F. *Biomacromolecules* **2003**, *4*, 987.
- (7) (a) Wang, S.; Advincula, R. C. *Org. Lett.* **2001**, *3*, 3831. (b) Park, M.-K.; Advincula, R. C. *Langmuir* **2002**, *18*, 4532. (c) Patton, D.; Park, M.-K.; Wang, S.; Advincula, R. C. *Langmuir* **2002**, *18*, 1688. (d) Advincula, R. C.; Fells, E.; Park, M.-K. *Chem. Mater.* **2001**, *13*, 2870. (e) Wang, S.; Wang, X.; Li, L.; Advincula, R. C. *J. Org. Chem.* **2004**, *69*, 9073. (f) Advincula, R.; Park, M.-K.; Baba, A.; Kaneko, F. *Langmuir* **2003**, *19*, 654.
- (8) Park, M.-K.; Deng, S.; Advincula, R. C. *J. Am. Chem. Soc.* **2004**, *126*, 13723.
- (9) Locklin, J.; Shinbo, K.; Onishi, K.; Kaneko, F.; Bao, Z.; Advincula, R. C. *Chem. Mater.* **2003**, *15*, 1404.
- (10) (a) Shchukin, D. G.; Sukhorukov, G. B.; Mohwald, H. *Chem. Mater.* **2003**, *15*, 3947. (b) Berth, G.; Voigt, A.; Dautzenberg, H.; Donath, E.; Mohwald, H. *Biomacromolecules* **2002**, *3*, 579.
- (11) Caruso, F.; Schuler, C.; Kurth, D. G. *Chem. Mater.* **1999**, *11*, 3394.
- (12) (a) Park, M.-K.; Onishi, K.; Locklin, J.; Caruso, F.; Advincula, R. C. *Langmuir* **2003**, *19*, 8550. (b) Park, M.-K.; Deng, S.; Advincula, R. C. *Langmuir* **2005**, *21*, 5272. (c) Park, M.-K.; Xia, C.; Advincula, R. C.; Schutz, P.; Caruso, F. *Langmuir* **2001**, *17*, 7670.
- (13) (a) Wu, Y. L.; Li, Y. N.; Gardner, S.; Ong, B. S. *J. Am. Chem. Soc.* **2005**, *127*, 614. (b) Kuwahara, A.; Nakano, K.; Nozaki, K. *J. Org. Chem.* **2005**, *70*, 413. (c) Sanda, F.; Kawaguchi, T.; Masuda, T.; Kobayashi, N. *Macromolecules* **2003**, *36*, 2224. (d) Zhu, G. X.; Conner, S.; Zhou, X.; Shih, C.; Brooks, H. B.; Considine, E.; Dempsey, J. A.; Ogg, C.; Patel, B.; Schultz, R. M.; Spencer, C. D.; Teicher, B.; Watkins, S. A. *Bioorg. Med. Chem. Lett.* **2003**, *13*, 1231. (e) Meng, L. H.; Liao, Z. Y.; Pommier, Y. *Curr. Top. Med. Chem.* **2003**, *3*, 305.
- (14) (a) Diamant, Y.; Chen, J.; Han, H.; Kamenev, B.; Tsybeskov, L.; Grebel, H. *Synth. Met.* **2005**, *151*, 202. (b) Li, J. L.; Dierschke, F.;

- Wu, J. S.; Grimsdale, A. C.; Mullen, K. *J. Mater. Chem.* **2006**, *16*, 96. (c) Huang, J.; Niu, Y.; Xu, Y.; Hou, Q.; Yang, W.; Mo, Y.; Yuan, M.; Cao, Y. *Synth. Met.* **2003**, *135*, 181. (d) Tao, X. T.; Zhang, Y. D.; Wada, T.; Sasabe, H.; Suzuki, H.; Watanabe, T.; Miyata, S. *Adv. Mater.* **1998**, *10*, 226. (e) Rani, V.; Santhanam, K. S. V. *J. Solid State Electrochem.* **1998**, *2*, 99.
- (15) Iraqi, A.; Wataru, I. *J. Polym. Sci., Part A: Polym. Chem.* **2004**, *42*, 6041.
- (16) Schwendeman, I.; Hickman, R.; Sonmez, G.; Schottland, P.; Zong, K.; Welsh, D. M.; Reynolds, J. R. *Chem. Mater.* **2002**, *14*, 3118.
- (17) Jin, S. H.; Kim, W. H.; Song, I. S.; Kwon, S. K.; Lee, K. S.; Han, E. M. *Thin Solid Films* **2000**, *363*, 255.
- (18) Belloni, M.; Kariuki, B. M.; Manickam, M.; Wilkie, J.; Preece, J. A. *Cryst. Growth Des.* **2005**, *5*, 1443.
- (19) (a) Belletete, M.; Bouchard, J.; Leclerc, M.; Durocher, G. *Macromolecules* **2005**, *38*, 880. (b) Bouchard, J.; Belletete, M.; Durocher, G.; Leclerc, M. *Macromolecules* **2003**, *36*, 4624.
- (20) Ling, Q. D.; Song, Y.; Ding, S. J.; Zhu, C. X.; Chan, D. S. H.; Kwong, D. L.; Kang, E. T.; Neoh, K. G. *Adv. Mater.* **2005**, *17*, 455.
- (21) (a) Xia, C.; Advincula, R. *Chem. Mater.* **2001**, *13*, 1682. (b) Xia, C.; Fan, X.; Park, M.-K.; Advincula, R. C. *Langmuir* **2001**, *17*, 7893. (c) Inaoka, S.; Advincula, R. *Macromolecules* **2002**, *35*, 2426. (d) Taraneekar, P.; Fan, X.; Advincula, R. *Langmuir* **2002**, *18*, 7943. (e) Deng, S.; Advincula, R. C. *Chem. Mater.* **2002**, *14*, 4073. (f) Taraneekar, P.; Baba, A.; Fulghum, T. M.; Advincula, R. *Macromolecules* **2005**, *38*, 3679. (g) Taraneekar, P.; Park, J.; Patton, D.; Fulghum, T.; Ramon, G.; Bittner, E.; Advincula, R. *Adv. Mater.* **2006**, *18*, 2461. (h) Taraneekar, P.; Baba, A.; Park, J.; Fulghum, T.; Advincula, R. *Adv. Funct. Mater.* **2006**, *16*, 2000. (i) Taraneekar, P.; Fulghum, T.; Baba, A.; Patton, D.; Advincula, R. *Langmuir* **2007**, *23*, 908. (j) Ravindranath, R.; Ajikumar, P.; Baba, A.; Bahuleyan, S.; Hanafiah, N.; Advincula, R.; Knoll, W.; Valiyaveetil, S. J. *Phys. Chem. B* **2007**, *111*, 6336.
- (22) Waenkaew, P.; Taraneekar, P.; Phanichphant, P.; Advincula, R. *Macromol. Rapid Commun.* **2007**, *28*, 1522.
- (23) (a) Izumrudov, V.; Sukhishvili, S. A. *Langmuir* **2003**, *19*, 5188. (b) Ruths, M.; Sukhishvili, S. A.; Granick, S. J. *Phys. Chem. B* **2001**, *105*, 6202.
- (24) Jegadesan, S.; Advincula, R. C.; Valiyaveetil, S. *Adv. Mater.* **2005**, *17*, 1282.
- (25) Fulghum, T.; Karim, S. M. A.; Baba, A.; Taraneekar, P.; Nakai, T.; Masuda, T.; Advincula, R. C. *Macromolecules* **2006**, *39*, 1467.
- (26) Taraneekar, P.; Fulghum, T.; Patton, D.; Ponnampati, R.; Clyde, G.; Advincula, R. *J. Am. Chem. Soc.* **2007**, *129*, 12537.
- (27) Hibbert, D. *Introduction to Electrochemistry*; Macmillan: New York, 1993; p 350.
- (28) (a) Moller, S.; Perlov, C.; Jackson, W.; Taussig, C.; Forrest, S. R. *Nature (London)* **2003**, *426*, 166. (b) Wang, Y. H.; MasPOCH, D.; Zou, S. L.; Schatz, G. C.; Smalley, R. E.; Mirkin, C. A. *Proc. Natl. Acad. Sci. U.S.A.* **2006**, *103*, 2026. (c) Hiller, J.; Mendelsohn, J. D.; Rubner, M. F. *Nat. Mater.* **2002**, *1*, 59. (d) Cui, X. D.; Primak, A.; Zarate, X.; Tomfohr, J.; Sankey, O. F.; Moore, A. L.; Moore, T. A.; Gust, D.; Harris, G.; Lindsay, S. M. *Science* **2001**, *294*, 571. (e) Lee, J.; Lientschnig, G.; Wiertz, F.; Struijk, M.; Janssen, R. A. J.; Egberink, R.; Reinhoudt, D. N.; Hadley, P.; Dekker, C. *Nano Lett.* **2003**, *3*, 113. (f) Austin, M. D.; Chou, S. Y. *Nano Lett.* **2003**, *3*, 1687.
- (29) Jegadesan, S.; Sindhu, S.; Advincula, R. C.; Valiyaveetil, S. *Langmuir* **2006**, *22*, 780.
- (30) Jegadesan, S.; Taraneekar, P.; Sindhu, S.; Advincula, R. C.; Valiyaveetil, S. *Langmuir* **2006**, *22*, 3807.
- (31) Jiang, G.; Baba, A.; Advincula, R. *Langmuir* **2007**, *23*, 817.
- (32) (a) Yoo, D.; Shiratori, S. S.; Rubner, M. F. *Macromolecules* **1998**, *31*, 4309. (b) Shiratori, S. S.; Rubner, M. F. *Macromolecules* **2000**, *33*, 4213.
- (33) Glinel, K.; Moussa, A.; Jonas, A. M.; Laschewsky, A. *Langmuir* **2002**, *18*, 1408.
- (34) Lyuksyutov, S. F.; Vaia, R. A.; Paramonov, P. B.; Juhl, S.; Waterhouse, L.; Ralich, R. M.; Sigalov, G.; Sancaktar, E. *Nat. Mater.* **2003**, *2*, 468.
- (35) Baba, A.; Locklin, J.; Xu, R.; Advincula, R. *J. Phys. Chem. B* **2006**, *110*, 42.
- (36) Xie, X. N.; Deng, M.; Xu, H.; Yang, S. W.; Qi, D. C.; Gao, X. Y.; Chung, H. J.; Sow, C. H.; Tan, V. B. C.; Wee, A. T. S. *J. Am. Chem. Soc.* **2006**, *128*, 2738.
- (37) Bo, Z.; Zhang, W.; Zhang, C.; Shen, J. *Macromol. Chem. Phys.* **1998**, *199*, 1323.

MA800268N